Hybrid Network Structure and Mechanical Properties of Rodlike Silicate/Cyanate Ester Nanocomposites

Yongzheng Pan,[†] Yue Xu,[†] Li An,[†] Hongbin Lu,*[,†] Yuliang Yang,*[,†] Wei Chen,[‡] and Steven Nutt[‡]

The Key Laboratory of Molecular Engineering of Polymers, Ministry of Education, and Department of Macromolecular Science, Fudan University, Shanghai 200433, China, and Department of Chemical Engineering and Materials Science, University of Southern California, Los Angeles, California 90089-0241

Received April 13, 2008; Revised Manuscript Received October 7, 2008

ABSTRACT: Silicate nanorods (attapulgite, ATT) were organically modified and homogeneously dispersed in a cyanate ester (CE) resin. ATT dispersions and networks were characterized by rheological and microscopic measurements. Amine groups grafted onto the particle surface catalyzed the cyclotrimerization of the CE monomers and enabled the CE monomers to enter the inter-rod spacing of loose aggregates easily, resulting in homogenization of the particle size distribution in the nanocomposites. The addition of nanorods decreased the density of organic networks and increased intracyclizations. Covalent bonding at the interface was confirmed by Fourier transform infrared (FTIR) spectroscopy and dynamic mechanical analysis (DMA), which establishes a basis for enhancing/optimizing mechanical properties of CE resins. Nanocomposite modulus, strength, and toughness increased 40, 42, and 55%, respectively, relative to the neat resin, although high nanorod loadings (e.g., 8 wt %) showed negligible benefit. The interplay between nanorod and resin networks governed the mechanical properties of the nanocomposites. The curing reaction decreased the size of particle aggregates and thus reduced the percolation threshold of particle networks. Particle networks induced the formation of more linear or branching polymer molecular structures, resulting in weaker particle−matrix interactions. These factors reduced the stress transfer efficiency and crack propagation resistance, impairing the extent of reinforcing at high particle loadings.

1. Introduction

The addition of inorganic nanoparticles to polymers can form hybrid organic−inorganic networks, provided the particle loading exceeds the critical volume fraction. The resulting nanocomposite can exhibit enhancements in thermal, mechanical, and functional properties.[1−4] For example, a transparent nanomembrane composed of ZrO_2 hybrid networks reportedly supported a load that was 70 000 times its own weight but was sufficiently flexible to pass a hole that was 30 000 times smaller than its own size;[2] hydrogels containing exfoliated clay hybrid networks displayed nearly complete strain recovery and a rapid deswelling response to temperature changes.[3] In addition, hybrid networks were shown to have markedly reduced flammability and improved processing characteristics.[4] These studies demonstrate that hybrid networks have opened a promising route for optimizing polymer performance, although efficient use of this route requires fundamental understanding to control the formation of hybrid networks and exploit the synergy between organic and inorganic networks.

To create and exploit hybrid networks in polymer composites, nanoparticles with spherical,[1,5] fibrous,[6] and platelike[3,7] particle shapes have been produced and studied. The studies reveal that the particle geometry and dispersion control the structure of inorganic networks.[8] Increasing aspect ratio generally reduces the percolation thresholds for a wide range of suspensions and nanocomposites, a phenomenon that has been theoretically analyzed.[8,9] Aggregated nanoparticles normally elevate the percolation threshold, thereby diminishing interfacial interaction and the contribution to bulk properties. In this regard, a general strategy for nanoparticle dispersion in polymers has been suggested in which an entropically unfavorable dispersion can be offset by an enthalpy gain arising from increasing molecular contacts. Stated differently, nanoparticle dispersions can be improved by the selection of polymers with radii of gyration that are greater than the particle size.[10]

Nanoparticles in mixtures also alter the reaction kinetics of organic components and the resulting network structure. This is of particular importance for systems that involve curing reactions or the simultaneous formation of organic/inorganic networks. Experimental observations have shown two opposite tendencies: the addition of nanoparticles may either accelerate or retard the curing kinetics.[11] For example, the addition of organically modified layered silicates reportedly decreased the cure time of UV-curable polymer systems because of the suppressed termination reaction; furthermore, the reduction in cure time became more significant when a single long chain was tethered to the silicate surface.[12] The trend is qualitatively consistent with model simulations in which the effect of linker length, tether rigidity, and reactive tether number on the extent of cross-linking has been examined.[13] The opposite tendency (retarded cure kinetics) was observed when colloidal silica particles were added to UV-curable thiol-ene systems, even though the reaction mechanism was not altered.[14]

In addition, the interface structure of organic/inorganic hybrid networks can affect bulk properties. The optimization of nanocomposite strength largely depends on the load transfer efficiency between hard inorganic networks and soft organic matrices.[15] Achieving optimal mechanical reinforcement requires effective interface bonding, which results from maximizing bond density and entanglements between near-field (the interface) and far-field (the bulk) molecules.[16]

These experimental and theoretical studies reflect the complexity in controlling the formation of hybrid networks, which is nonetheless necessary to optimize nanocomposite properties. Despite a large volume of literature, a complete understanding of the correlation between hybrid networks and macroscopic properties of nanocomposites remains elusive. A key issue arises

* Corresponding authors. E-mail: hongbinl@fudan.edu.cn, yuliangyang@fudan.edu.cn.
[†] Fudan University.
[‡] University of Southern California.

10.1021/ma800819s CCC: $40.75
Published on Web 11/11/2008

from the fact that the addition of nanoparticles normally increases the mixture viscosity, which inevitably affects the mechanism of hybrid network formation and alters the response to applied forces and thermal fields. This constitutes the primary motivation of the current work, in which we explore the effect of rodlike nanoparticles on the viscosity of precursor resins (a bisphenol A cyanate ester resin), the cure reaction, the hybrid network formation, and the resulting mechanical properties.

Rodlike nanoparticles exhibit distinctive geometric characteristics and have received widespread attention.[17] As functional additives, they have been exploited to make very efficient polymer solar cells that rely on the rapid charge transfer rates along the nanorods.[17d] Nanorods have also been used as reinforcing fillers.[17c] For example, the addition of 15.5 vol % cellulosic whiskers increased the shear modulus of polybutadiene composites by over 2 orders of magnitude.[18] Compared with other anisotropic nanoparticles, for example, layered silicates, rodlike nanoparticle morphologies are readily controlled, without one having to worry about the intercalation or exfoliation kinetics, as in layered silicate particles.[16b,17e,19] This is beneficial not only for controlling nanocomposite structure and morphologies but also for elucidating fundamental issues. Using rodlike ATT silicates, we have demonstrated the influence of multiple factors, including particle network, interfacial interaction, and free volume on the strength, toughness, and thermal stability of thermoplastic polymer nanocomposites.[16b] Here we extend our studies to a thermosetting system and explore the formation of hybrid networks and associated structure−property relationships.

Cyanate esters (CEs) are thermosetting resins with processing characteristics similar to those of epoxy resins, thermal stability similar to that of bismaleimides, and flame resistance similar to that of phenolic resins and are widely used in electronic and aerospace applications.[20] They are cured to heterocyclic phenolic triazine networks by cyclotrimerization with or without catalysts. CEs tend to be brittle, a factor that often restricts structural applications.[21] As a result, toughening has been pursued via structural modification,[21]a blending with rubbers or thermoplastic inclusions,[21b,d,e,g,h] and the incorporation of inorganic particles.[21c,f] The particle-toughening approach is often selected because of the favorable performance−cost ratio and processability.[5a,22] For example, Che and Chan-Park demonstrated prominent strength and toughness improvements by adding single-walled carbon nanotubes in CE resins.[22a] Nevertheless, the understanding of the resulting hybrid network structures in CE nanocomposites and their correlation with macroscopic properties is far from complete.

In this work, organic modification of rodlike nanoparticles is employed to improve the dispersion stability in CE monomers, and an effort is undertaken to correlate the microstructure with mechanical properties of nanocomposites. The formation and evolution of organic networks is monitored in situ by thermal analysis and spectroscopic techniques. Relevant strengthening and toughening mechanisms are proposed on the basis of variations in network density, stress transfer efficiency at the interface, and free volume fraction introduced by nanoparticles.

2. Experimental Section

2.1. Materials. Bisphenol A dicyanate (HF-1, melting point: 80 to 82 °C, purity ≥99.0%) with a cyanate equivalent of 139 g/equiv (Shanghai Huifeng Technology and Business) was used as the resin formulation. Attapulgite (ATT) (Attagel 50, Engelhard) was acquired, and 4,4′-diaminodiphenylmethane (MDA) and 4,4′-methylenebis(phenylisocyanate) (MDI) were purchased (Sigma-Aldrich Chemical) and used as received. *N*,*N*-dimethylformamide (DMF) was distilled in vacuum over anhydrous magnesium sulfate. All other reagents and chemicals were analytical grade and were used without purification.

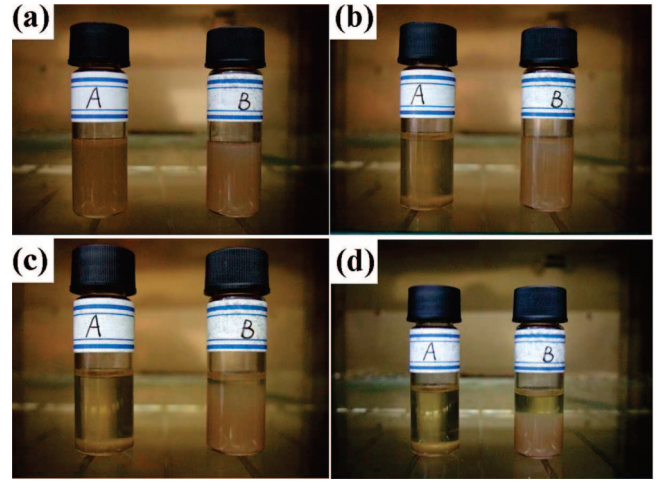

Figure 1. Dispersion of 2 wt % organically modified ATT nanorods in CE monomer at an observation temperature of 90 °C at (a) 0, (b) 2, (c) 4, and (d) 8 h.

2.2. Sample Preparation. *4,4′-Diaminodiphenylmethane-Modified Attapulgite Nanorods.* Attapulgite (ATT) clay is a kind of natural magnesium aluminum silicate that is often used as Maya blue paint in Mesoamerica and exhibits a characteristic rodlike morphology.[16b,c,19] A single ATT nanorod is approximately 20 nm in diameter and several micrometers in length.[16d] These nanorods tend to be bundled together in natural minerals because of the presence of impurities such as carbonates, illite, quartz, and so on. The removal of impurities contributes to the exfoliation of ATT bundles. As-received ATT particles have had their impurities largely removed by various techniques such as grinding/milling and sedimentation;[16e] however, it was found in our work that a small amount of non-ATT particles and large aggregates still exists in the acquired ATT powder. To eliminate these impurities and aggregates, a purification procedure was also included in the organic modification of ATT nanorods.

ATT powder was first dispersed in sodium hexametaphosphate solution at 50 °C with the assistance of high shearing and ultrasonication. After centrifugation, the supernatant suspension was collected. The purified ATT was subsequently activated in 5 M HCl solution at 80 °C for 1 h to remove the residual impurities and to introduce hydroxyl groups on the surface. After exhaustive washing with water to pH neutral, the activated ATT were dried at 150 °C under vacuum for 24 h. The dried ATT (5 g) was ground and redispersed in dry DMF to form a 5 wt % suspension with a high-shear homomixer and ultrasonication. MDI solution in DMF (0.01 mol) was added to the ATT suspension with vigorous stirring. The mixture was maintained at 80 °C under nitrogen for 1 h to complete the reaction between isocyanate and hydroxyl groups. After washing twice with DMF, a solution of MDA (0.05 mol) in DMF was added and stirred at 55 °C overnight for the reaction between isocyanate and amine groups. The modified ATT was collected by centrifugation at 6000 rpm. To remove ungrafted molecules exhaustively, the modified ATT was washed sequentially with DMF, water, and acetone and was then dried in a vacuum oven.

Attapulgite/Cyanate Ester Nanocomposites. The CE monomer was placed in a flask in an oil bath and was melted at 90 °C to obtain a low viscosity liquid. After measured quantities of modified ATT were added to the CE liquid, a high-shear mixing blade was used to stir the mixture at 10 000 rpm for 20 min. The mixing process was repeated three times, and the mixtures were subsequently degassed for 1 h in a vacuum oven at 90 °C. Parts of mixtures were removed for spectroscopic and rheological characterization, and the remainders were poured in molds to prepare samples for thermal analysis, microscopy, and measurement of mechanical properties. The cure cycle for all samples was identical:

170 °C for 2 h, 200 °C for 2 h, and 240 °C for 1 h, then naturally cooling to 20 °C.

4,4′-Diaminodiphenylmethane/Cyanate Composites. The CE monomer was placed in a flask in an oil bath and was melted at 90 °C, to which different amounts of MDA (0.6, 1.2, and 2.4 wt %) were added. The mixtures were stirred at 90 °C until the MDA was completely dissolved in the CE monomer. Similarly, parts of mixtures were extracted and cooled to room temperature for characterization, and the remainders were poured in molds and cured following the same curing cycle as that used for the nanocomposites.

2.3. Measurements and Characterization. Differential scanning calorimetry (TA Q100, DSC) was used to monitor the curing reaction of the neat resin and ATT/CE mixtures. Samples were heated at 10 °C/min from 50 to 380 °C under a nitrogen flow of 50 mL/min. The extent of cure was evaluated by reheating samples under the same conditions (50 to 380 at 10 °C/min) and integrating the exothermal peak area to calculate the reaction heat. The glass transition temperatures (T_g) of the neat resin and ATT/CE nanocomposites were also measured by DSC. To diminish the effects of uncompleted reactions and thermal history, all samples were first heated from 50 to 350 at 20 °C/min and were held at 350 °C for 5 min. After cooling to 50 °C at the same rate, all samples were reheated to 350°C at 20 °C/min. The process was completed with a N_2 purge at 50 mL/min.

In-situ Fourier transform infrared (FTIR) spectroscopy was performed on an infrared spectrophotometer (Nicolet Magna-470) equipped with a temperature-controlled sample holder in a N_2 atmosphere. The uncured samples were placed between two NaCl salt plates, and spectra were obtained in an optical range of 650 to 4000 cm^{-1} using an average of 32 scans and a resolution of 4 cm^{-1}.

Rheological measurements of ATT/CE suspensions were conducted on a rheometer (Haake RS-75) at 90 °C, using a 60 mm diameter cone−plate fixture. Samples were mixed for 30 min and stabilized at 90 °C for 15 min prior to tests. Samples (3 mL each) were placed between the cone and plate of the rheometer. The gap size of the cone−plate was adjusted to 0.108 mm, and the measuring temperature was maintained at 90 °C. For each sample, a stress-controlled rotation ramp and a stress-controlled oscillation frequency sweep were conducted. The flow curve was created with a stress-controlled rotation ramp, beginning with an initial stress of 0.02 Pa. The stress sweeps were halted when the shear rate approached 1000 s^{-1}. The oscillation frequency sweeps were performed in a frequency range of 0.1−10 Hz with an applied stress of 0.1 Pa.

The chemorheological behavior of the neat resin and ATT/CE mixtures was studied under an isothermal curing condition by using a rheometer (Haake RS-75). A parallel plate fixture (20 mm diameter) was employed. All samples were mixed for 30 min and stabilized for 15 min at 90 °C prior to testing. About 0.5 mL of each sample was placed between two parallel plates of the rheometer, and the gap size was adjusted to 1 mm. All samples were measured with a 1 Hz frequency at 170 °C to monitor the isothermal gelation behavior by the oscillation time sweep mode. The imposed stress for these experiments was 2 Pa.

Microscopic observations were performed on a transmission electron microscope (TEM, Hitahi 600) and a scanning electron microscope (SEM, Philip 30). To determine dispersions in the organic solvent (DMF), modified ATT nanorods (0.69 and 2.0 g/mL) were added to the DMF, were highly sheared (with a high shearing mixer) for 30 min, and were then ultrasonicated for 15 min. Nanorods in the suspensions were collected on copper grids for TEM observation. For cured resin and nanocomposite samples, thin sections (∼70 μm) were prepared using a microtome. Fracture surfaces of the neat resin and nanocomposites were observed by SEM (TESCAN 5136MM) after gold coating. All samples were etched with 6 M HCl solution at room temperature for 10−15 min before gold coating.

Flexural properties were measured using a universal testing machine (CMT-4102, SANS Group, China). A three-point bend fixture was used, and all measurements were conducted at room temperature with a crosshead speed of 1 mm/min. At least four specimens for each material were tested following an ASTM standard (ASTM-D790) with a sample dimension, 30 × 6 × 2 mm^3. Flexural strength, σ_f, was calculated in terms of eq 1

$$\sigma_f = \frac{3FS}{2wd^2} \tag{1}$$

where F is the applied force at the breaking point, S is the span between two fulcrums (20 mm), w is the specimen width, and d is the specimen depth. Flexural modulus, E_f, was calculated using eq 2

$$E_f = \frac{\Delta F S^3}{4wd^3} \tag{2}$$

where ΔF is the slope in the linear region of the force−deformation curve.

Fracture toughness (K_{IC}) was measured with a crosshead speed of 0.5 mm/min using single-edge-notched (SEN) specimens with a dimension of 30 × 6 × 2 mm^3. K_{IC} was calculated using eq 3

$$K_{IC} = Y\frac{3FS\sqrt{a}}{2wd^2} \tag{3}$$

where Y is a shape factor with $Y = 1.93 - 3.07(a/d) + 14.53(a/d)^2 - 25.11(a/d)^3 + 25.80(a/d)^4$ and a is the crack length.

Dynamic mechanical analysis (DMA) was performed (Netzsch DMA 242) using a single cantilever clamp under the following conditions: temperature range of 50−330 °C, frequency of 1 Hz, and heating rate of 5 °C/min. Thermogravimetric analysis (TGA) was conducted (Perkin-Elmer Pyris 1 TGA) with a temperature range of 50−800 °C, a heating rate of 20 °C/min, and a N_2 flow rate of 40 mL/min.

3. Results and Discussion

3.1. Dispersion and Particle Networks of Attapulgite in Cyanate Ester. Performance optimization of polymer nanocomposites requires homogeneous dispersion of nanoparticles. In a previous work,[16b] an aromatic diisocyanate (MDI) was used to capture surface hydroxyl groups on ATT nanorods, and amine groups were then introduced to the nanorod surface by reacting with an aromatic diamine (MDA). This modification improved the dispersion of nanorods in organic solvents and polyamic acid solutions. The same protocol is used here to achieve a homogeneous dispersion of ATT in the CE resin, exploiting the reactivity of aromatic amines with CE groups, the thermal stability under curing conditions, and the catalytic effect on the CE cure reaction. The images in Figure 1, which were recorded at 90 °C, illustrate the stability of the dispersion of modified nanorods in the CE monomer (melting point: ∼80 °C, weight fraction: 2 wt %). Unmodified ATT nanorods naturally settle in the CE monomer (because of the density difference), and complete sedimentation occurs in 2 h. In contrast, the MDA-modified nanorod suspension shows no discernible sedimentation in 2 h. The sedimentation rate is so slow that a thin layer of supernatant appears only after 4 h. In the lower half of the vial, a concentration gradient exists in which the particle concentration increases near the bottom. The concentration gradient persists even after 8 h, although the packing of nanorods becomes denser with time. The surface modification approach effectively improved the dispersion stability of nanorods in the CE monomer. This is important for the subsequent thermal cure of nanorod/CE mixtures, especially given the relatively low viscosity of the CE monomer (only ∼10 mPa·s at 90 °C; nearly an order of magnitude lower than that of common bisphenol A epoxy resins such as Epon 828).

Three possible causes are considered for the stable dispersion of nanorods in CE monomer. First, the organic molecules grafted onto the particle surface may enhance the solvation interaction of nanorods and monomers. Generally, the solvation interaction

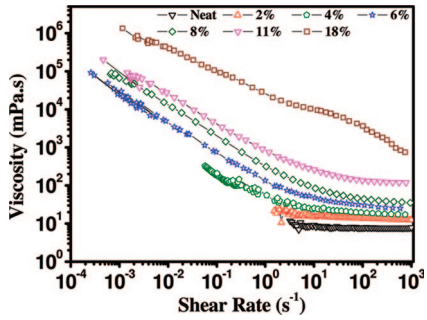

Figure 2. Steady-state rheological experiments under stress control modes. Viscosity versus shear rate for the CE monomer and mixtures with different nanorod contents. Imposed initial stress: 0.02 Pa, shear rate: $2 \times (10^{-4}-10^{3})$ s^{-1}.

between particles and dispersing media increases with increasing size of grafting molecules or increasing reaction probability with the medium.[23] However, the molecular size of MDI and MDA in the present work is unlikely to stabilize the ATT nanorods, which are tens of nanometers in diameter and microns in length. Nevertheless, the chemical structure of the grafts is similar to the CE monomer, which undoubtedly increases the miscibility between the nanorods and the monomer, especially after surface amine groups react with CE monomers, as discussed later. Second, the increased viscosity of the suspension may retard sedimentation and stabilize the dispersion. Anisotropic nanoparticles normally exhibit a larger flow resistance than spherical nanoparticles, which limits sedimentation.[24] Finally, percolated particle networks help to stabilize the suspension, particularly when the particle content exceeds the percolation threshold. This has been observed in rheological measurements of suspensions containing layered silicates, carbon nanotubes, and POSS.[25] Although the particle content in our sedimentation experiments (2 wt %) may be less than the critical percolation threshold, once percolated networks form, higher nanorod contents will retard the sedimentation and stabilize the dispersion.

Rheological characterization revealed characteristics of the network structure in both monomer suspensions and nanocomposites. Figure 2 shows the effect of nanorod content on the steady-state viscosity of ATT/CE mixtures. The measurements were performed at 90 °C with an initial stress of 0.02 Pa. The neat CE resin is a Newtonian fluid (viscosity independent of shear rate). The addition of ATT nanorods caused the viscosity of suspensions to increase in increments that became larger at higher loadings. At particle loadings of greater than 2 wt %, shear-thinning (thixotropic behavior) was observed. Similar observations have been reported for suspensions and dispersions involving different particle morphologies,[25] reflecting the existence of particle networks (at high loadings) or floc structures (at low loadings). Although models have been presented to describe the steady-state rheological behavior of thixotropic fluids,[26a,b] application to the current ATT/CE dispersions does not yield an appropriate percolation threshold for nanorods in the CE monomer, which drives us to consider other approaches.

Dynamic experiments for the dispersing systems were conducted at 90 °C to determine the percolation threshold of nanorods in the CE monomer. According to Winter and Chambon,[26c] the dynamic storage and loss moduli of both chemical and physical gel systems follow a simple power law at the critical gel point: $G'(\omega) \approx G''(\omega) \sim \omega^{n}$, which means that the loss tangent (tan δ) at this point is independent of the frequency. The criterion has been used in some gels[26d] and is extended at present to ATT/CE mixtures. Figure 3 shows the frequency dependence of tan δ for different ATT/CE mixtures, suggesting a percolation threshold of 9.0 wt %. (The dynamic storage and loss moduli of ATT/CE mixtures clearly exhibit a

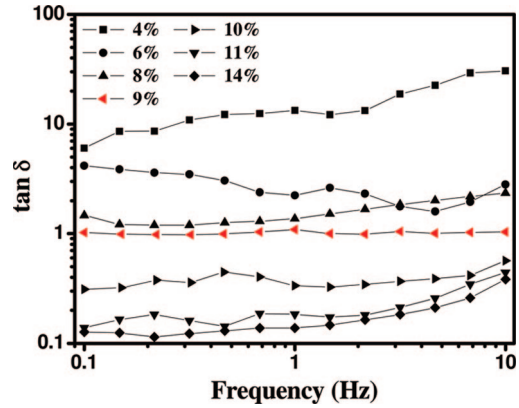

Figure 3. Dynamic rheological experiments under stress control modes: loss tangent (tan δ) versus frequency for ATT/CE monomer mixtures with different nanorod contents. Imposed stress: 0.1 Pa, frequency: 0.1−10 Hz.

solidlike behavior with increasing ATT contents; see Figures S1 and S2 in the Supporting Information.) The ATT nanorods used here exhibit an aspect ratio of ~18.[16b] Using a Padé-type approximation ($1/\phi_c = (7.742 + 14.61x + 12.33x^{3/2} + 1.763x^2 + 1.658x^3)/(9.875x + x^2)$, where ϕ_c is the critical volume fraction and x is the aspect ratio), a value of $\phi_c = 5.90$ wt % is obtained. The discrepancy between predicted and measured values of ϕ_c can be attributed to the presence of aggregates in the CE dispersions, a phenomenon that is next investigated.

Figure 4 shows the dispersions of nanorods in organic solvent (DMF) and in cured CE resins. Because of the difficulty in preparing TEM samples of ATT/CE monomer mixtures, we directly observed the dispersion of ATT nanorods in DMF as opposed to the CE monomer. The ATT nanorods were dispersed in DMF (0.69 mg ATT/mL DMF) by high shearing (0.5 h) and ultrasonication (15 min) before being placed on copper grids. A small number of large aggregates (microns) were observed, as shown in the inset of Figure 4A. The majority of particles appeared in small aggregates containing two or several individual nanorods (Figure 4A). Diameters ranged from 80 to 300 nm and lengths ranged from 500 nm to 3 μm. Small aggregates appear to originate from accompanying impurities such as carbonates, illites, and so on. These impurities may link ATT nanorods together. Normally, these impurities are difficult to remove completely, and as a result, such small aggregates may persist in CE resins even after curing. Alternatively, two different amino-substituted rods could react with a single tricynate molecule, linking two nanorods together. Such reactions cannot be completely ruled out, although they are considered to be less likely. When a tricyanate molecule is grafted on the nanorod surface, the residual cyanate groups will be restricted in the vicinity of the nanorod. Compared with free tricyanate molecules in the system, the grafted cyanate groups possess lower mobility and probability of reacting with those amine groups tethered to other nanorods. This implies that the reaction probability of two restricted groups should be lowest relative to those reactions that involve free cyanate groups. The linkage of two nanorods can occur unless a tricyanate molecule happens to be in the vicinity of two grafted amine groups. Considering that in the current work a long-time high-shearing mixing (60 min) was imposed after the amino-substituted nanorods were added to the CE monomer, it should be reasonable to attribute the observed aggregates to the presence of residual impurities.

Larger agglomerates should diminish in size with further stirring or ultrasonication. In the 4 wt % nanocomposites, nanorods were better dispersed than in DMF, and large aggregates were rarely seen. Note that the shearing time for

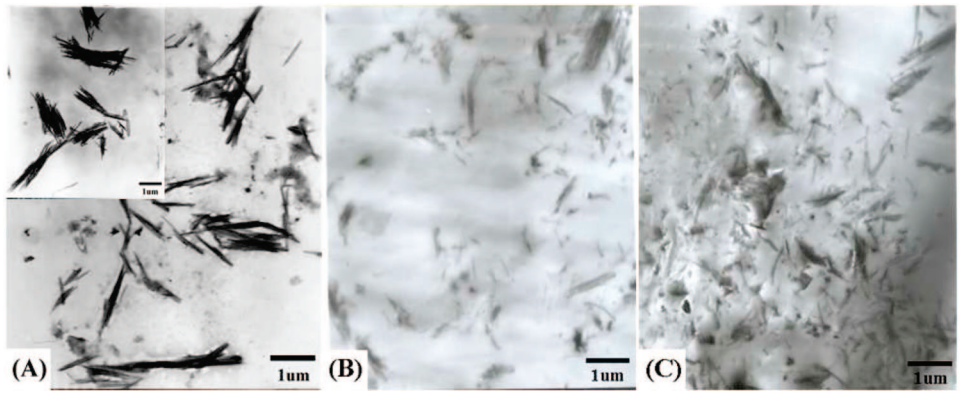

Figure 4. Network structures and particle aggregates formed in (A) organic solvent (DMF) and ATT/CE nanocomposites: (B) 4 wt % ATT and (C) 8 wt % ATT. The inset in A shows the nanorod aggregates observed under the condition identical to A.

dispersing ATT nanorods in the CE monomer was longer (3 × 20 min), and the CE monomer has greater miscibility with the grafting molecules, both of which contribute to improved dispersion. In addition, as later shown, during mixing at 90 °C, the grafting molecules can react with the cyanate group, thereby increasing the inter-rod distance. Large aggregates were more frequent in the 8 wt % sample, although they were much smaller than those in DMF. The loose agglomerates observed in DMF disappeared in the nanocomposites, and the size distribution of rodlike particles became more homogeneous (typical particle diameters were ~100 nm). Although it is difficult to determine the aspect ratio of ATT nanorods in cured CE resins, because some nanorods are fractured by the microtome, the observed morphologies are consistent with the increased percolation threshold that is observed in the rheological experiments.

The number of large aggregates in the nanocomposites increased with increasing particle loadings. To explore the concentration dependence, we prepared a high content ATT/DMF suspension (2.0 mg ATT/mL DMF), and larger agglomerates were indeed observed (not shown here). The rodlike nanoparticles tend to self-organize in parallel configurations because of a depletion interaction between nanorods.[17j] The latter arises from the reduction of the exclusion volume of nanorods in a mixture system, which is maximized as nanorods arrange themselves in some ordering form.[17] In related systems, nematic and smectic liquid crystalline phases for anisotropic nanorods reportedly occur, provided that the concentration in solution is greater than a threshold level and that a mobility requirement is met.[17g,27] Therefore, the increased aggregates observed in the 8 wt % sample can be attributed to a depletion interaction arising from the reduced separation between proximate nanorods at high loadings. Nevertheless, the differences in size and density of the agglomerates/aggregates observed in DMF (loose and large) and in CE resins (dense and small, Figure 3C) suggest alternative explanations. The concentration of the high-content ATT/DMF suspension is only 0.21 wt %, which is far less than the 4 and 8 wt % of nanocomposites. The morphology in DMF reflects not only the aggregating tendency of ATT nanorods in DMF but also the weaker dispersing capacity of DMF for nanorods compared with that for the CE monomer. Recall that in layered nanoparticle/polymer nanocomposites, both theoretical simulations and experiments suggested that the interplay of entropic and energetic factors determined the dispersion status of layered particles in matrices.[28] The entropic penalty of grafting molecules on particles may be compensated by the increased conformational freedom with increasing interparticle distances. Consequently, the dispersion status of layered particles in polymers largely depends on the affinity of polymer chains or monomers for particles, which may result in the appearance of different morphologies, including intercalated, exfoliated, and flocculated structures.

On the basis of this understanding, we assert that the large nanorod agglomerates observed in ATT/DMF suspensions primarily originate from the weak affinity and solvation effect of DMF for the nanorods. For homogeneous dispersion in the nanocomposites, the greater affinity of grafting molecules for the CE monomer allowed CE monomers to situate within the inter-rod spacing. Subsequent chain growth during curing further enlarged the inter-rod distance and led to the observed homogeneous dispersion. Careful comparison of the structures of ATT aggregates in DMF suspensions and nanocomposites revealed that the aggregates in suspensions were less dense relative to the nanocomposites. This implies that loosely packed ATT aggregates have been exfoliated during curing, but for dense aggregates, exfoliation needs higher energy because of the stronger adhesive forces between nanorods. It is consequently concluded that the cure reaction contributes to the breaking up of loose ATT agglomerates; the increase in the dense aggregates observed in the nanocomposites with high loadings (e.g., 8 wt % sample) is a statistical result; that is, higher particle contents caused an increase in the quantity of impurity-connected hard aggregates.

The results demonstrate the strong effects of surface modification and cure reactions on the dispersion of ATT nanorods in CE resins. The strong affinity of the grafting molecule for the medium enables the CE monomer to intercalate into the inter-rod spacing and significantly enlarges the distance between contiguous nanorods. This results in the homogeneous dispersion of nanorods in the nanocomposites. Although the percolation threshold of ATT/CE monomer suspensions is estimated at 8.5 wt %, this value might be high. The nanorod dispersion after subsequent curing reactions improves, which suggests the existence of a percolated network in the 8 wt % nanocomposite. We next consider the effects of nanorods on the formation of organic networks.

3.2. Effect of Attapulgite Nanorods on Cyanate Ester Networks. Thermal curing of CE monomers generates crosslinked polycyanurates via polycyclotrimerization of the OCN group. Lewis acids, transition metal complexes, and amines can be used to catalyze the cure reaction of CEs.[20] Recent work has shown that organically modified layered silicates have a catalytic effect on the cyclotrimerization. In particular, a decrease of 84 °C in exothermic peak temperature T_p was observed for a sample with 5 wt % layered silicates.[29] The authors determined that degradation of quaternary ammonium on the silicate surface first released a tertiary amine and produced a secondary amine, both of which catalyzed the curing reaction of CE monomers.

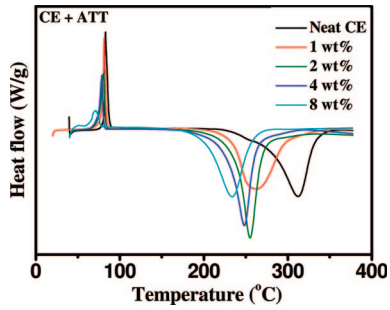

Figure 5. DSC curves during the cure reactions of ATT/CE and MDA/CE mixtures under the same conditions: 50−380 °C at 10 °C/min and a nitrogen flow of 50 mL/min.

Table 1. Cure Reaction Characteristics and Thermal Properties of Neat Ce and Nanocomposites with Different Loadings

sample	cure peak temperature T_p, °C	cure enthalpy ΔH, J/g	T_g by DSC, °C	T_d at 10 wt % weight loss, °C	gel time, min
neat CE	312	674.8	280	476	84
1 wt %	263	706.3	284	470	66
2 wt %	255	660.0	282	475	55
4 wt %	248	655.1	259	472	33
8 wt %	234	643.0	252	467	16

In the present system, primary amine groups are grafted onto the ATT surface; therefore, the ATT nanorods may exhibit a similar catalytic effect on the curing of the CE. Figure 5 shows DSC curves for neat CE and nanocomposites with different ATT loadings. The curves reveal a decrease in T_p (from 312 to 234 °C, or 78 °C) as well as a ~32 J/g decrease in cure enthalpy ΔH with increasing nanorod content. (See Table 1.) The enthalpy difference between the neat CE and 8 wt % nanocomposite is not significant and corresponds to a ~5% decrease relative to the ΔH of neat CE (675 J/g). Therefore, the addition of nanorods did not significantly affect the extent of cure of CE under the nonisothermal conditions employed (heating to 350 °C at 10 °C/min). However, the structure of CE networks may have been altered by the addition of the nanorods.

Chemorheological characterization was employed to probe the network formation of the CE resin. Figure 6 shows the effects of nanorods on G' and G'' of the neat CE and the CE/ATT mixtures (cure temperature: 170 °C, shear stress: 2 Pa), which allow us to track the evolution of organic networks and to determine the corresponding gel points of different systems. For the neat CE, an induction period of as long as 60 min can be seen in Figure 6A. In contrast, the incorporation of nanorods significantly reduced the induction periods. When the particle loading was greater than 4 wt %, induction times were difficult to determine because of the sharply increasing G''. After G'' exceeds 10 Pa, the variation in G' can be observed. A crossover point appears in the gelation region (increasing G' and G''), and this provides an indicator of gel time. Gel times for all samples are summarized in Table 1. The addition of ATT nanorods markedly reduced the gel time of CE resins from 84 min for the neat resin to 16 min for the 8 wt % nanocomposite. This trend resembles observations reported for CE nanocomposites containing layered silicates,[30] where the shortened gel time was attributed to the catalytic effect of quaternary ammonium cations grafted to the silicate surface.

To account for the effect of nanorods on the formation of organic networks, the same amount of primary amine (MDA) was homogeneously dispersed in CE monomers under the same condition to model the catalysis effect of aromatic amines grafted to the ATT surface on the cure reaction of CE resin. Figure 6B shows the effect of adding 0.6, 1.2, and 2.4 wt % of MDA on the rheological behavior of the CE resin during cure. (0.6, 1.2, and 2.4 wt % correspond to the amount of amine groups grafted on 2, 4, and 8 wt % ATT nanorods, respectively). The gel times for CE resins containing 0.6, 1.2, and 2.4 wt % MDA were 42, 21, and 12 min, respectively. More rapid gelation for CE/MDA systems relative to CE/ATT systems suggests that the ATT nanorods delayed the gelation of the CE resin. Further comparison of the G'' curves for the samples containing MDA versus those containing ATT nanorods revealed that the addition of ATT caused marked increases in G'' prior to the gel points. Apparently, increased viscous resistance retarded the diffusion-controlled cure kinetics of CE resins.

For thermosetting systems, the variation in the cure kinetics may alter the cross-link density of organic networks, which can be characterized by the T_g of systems. Figure 7 shows the DSC curves for CE resin with different ATT and MDA contents, from which the effect of nanorods and MDA on the T_g of CE networks can be determined. (See Table 1.) The T_g for the neat CE resin is 280.1 °C (manufacturer claims T_g > 260 °C). The addition of 2.4 wt % of MDA resulted in a slight decrease in T_g from 280.1 to 268.1 °C, which matches previous reports.[31] The increased segmental mobility has been attributed to the formation of dangling chain ends induced by cyanamides and released phenols. The latter reduced the branching density of networks because of the decreased number of triazine rings.[31] However, the effect of the addition of ATT with the same amine groups on the T_g of CE networks is different from the case in CE/MDA systems, in which a ~30 °C reduction in T_g is observed. The ATT causes a larger decrease in the network density, and the difference suggests that the system viscosity affects the formation of CE networks. This is not implausible for a diffusion-controlled cyclotrimerization involving the formation of triazine rings. The increase in viscosity inevitably causes a decrease in the diffusion rate of functional groups and thus limits the number of groups that take part in the reaction. Given the sample preparation protocols in the present work, the examination of the extent of completion of polycyclotrimerization for nanocomposites is warranted.

Figure 8 shows the DSC curves of samples after the curing procedure. All nanocomposites experienced further cure reaction after the temperature exceeded the T_g. However, the cure heats that were released during the further reaction were distinctly different for each sample. (See the inset of Figure 8.) Although the cure heats are small compared with the total cure heat that was released under the nonisothermal condition, the relative magnitudes reveal the viscosity effect of the cure reaction. For the neat CE, the uncompleted cure heat is 1.86 J/g, (the total cure heat was 674.8 J/g), indicating that the cure cycle nearly completed the reaction. Subsequent heating of the neat CE resin to 350 °C caused no change in T_g. In contrast, CE nanocomposites exhibited large differences in the cure heat and T_g. Lower ATT loadings (1 and 2 wt %) released higher cure heats compared with higher ATT loadings (4 and 8 wt %). Furthermore, both 1 wt % and 2 wt % samples displayed increases in T_g (close to the value of the neat resin) after heating to 350 °C. In contrast, the 4 and 8 wt % samples showed decreases in T_g after the same postcure.

These results highlight two points. First, the increases in T_g (for the 1 and 2 wt % ATT samples) caused by the postcure indicate that triazine rings are still available to form during reheating. This suggests that the viscosity increases associated with nanorod additions did not significantly retard the diffusion of cyanate groups at high temperatures; therefore, the CE network can be further consummated. Second, decreases in T_g (for the 4 and 8 wt % ATT samples) indicate that the formation of CE networks is influenced by multiple factors, including thermal history, viscosity, plasticization effects of released phenols, and possible intracyclization. The lower T_g values that

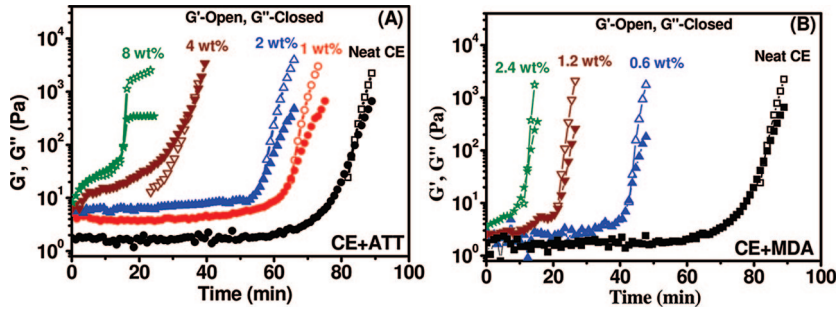

Figure 6. Chemorheological curves for CE resins with different ATT and MDA loadings under dynamic state conditions: static stress of 2 Pa and frequency of 1 Hz.

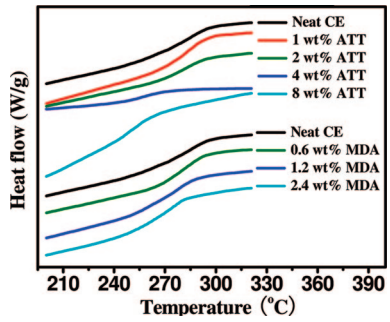

Figure 7. Comparison of T_g values for the neat resin, ATT/CE nanocomposites, and cured MDA/CE resins (obtained from the second scans after removing thermal history).

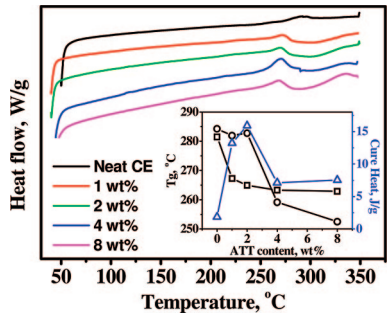

Figure 8. Residual reaction heats of samples with different ATT loadings: DSC scans after curing at different oven temperatures. In the inset: (□) T_g in the first scan, (○) T_g obtained in the second scan, and (Δ) residual cure heat.

result from reheating highlight the thermal history difference between the two cures. The first scan was conducted after relatively slow, natural cooling in an oven, which allows segments to rearrange and pack closely. In contrast, the second scan was performed after more rapid cooling, 40 °C/min, which affords less time for CE segments to pack efficiently and thus imparts more free space for segments to move. Nevertheless, the packing density difference is insufficient to explain the observed T_g decreases given that the neat resin showed no distinct difference between two scans. A more likely explanation is that because of increased system viscosity, the probability of functional group collisions decreased, which reduced the network density and the number of triazine rings. As shown in Figure 2, the viscosity of the mixtures rapidly increased with increasing nanorod loadings, especially at high ATT loadings. The viscosity will further increase as the cure reaction proceeds, thus limiting the formation of triazine rings. This assertion is consistent with the reduced cure heat observed in subsequent scans. Nevertheless, the decreased number of triazine rings should correspond to a reduced cure heat, which is inconsistent with the nearly unaffected reaction heat that was observed in nonisothermal experiments. (See Figure 5 and Table 1.) This leads us to conclude that other reactions (in addition to cyclotrimerization) contribute to the total reaction heat.

Intracyclization is a possible reason for the negligible changes in total reaction heats, which is an intramolecular cyclization of a given CE linear or monobranched chain in which triazine rings formed are not cross-link centers. This has been suggested by Wang and Hong as comparing the cure behavior of a dicyanate with rigid chain structure (DCSI) with that of a bisphenol A diacyanate (BADCy).[32] Because of its rigid structure, DCSI was expected to leave a high percentage of unreactive dicyanates in growing oligomers prior to gelation. However, the mass spectroscopic data from extraction experiments showed that when the conversion increased from 50 to 56%, the amount of trimer significantly decreased, and multiple peaks corresponding to molecular weights of monomer, dimer, trimer, tetramer, and pentamer appeared. This indicated that the reaction heat at high conversions primarily originated from the intracyclization of monomers or oligomers. The cyclotrimerization of cyanate groups is trimolecular and is different from two-body collisions and should thus deviate from the gel point (0.5) predicted by the mean field theory.[33] This is also consistent with the longer induction times observed in the CE nanocomposites relative to CE/MDA resins (Figure 6). Thus, the gel points of nanocomposites were delayed, and the probability of forming internal cycles increased.

Increasing the amount of monofunctional monomer elevates the probability of intracyclization.[31] For the CE nanocomposites, amine groups grafted onto the nanorod surface increased the fraction of monofunctional molecules resulting from the reaction between amine and cyanante groups. The reactivity of these grafting cyanate groups markedly decreases because of the restriction effect of nanorods. In the initial stage, cyclotrimerization is the dominant reaction, which is a consequence of large amounts of cyanate groups surrounding the nanorods. However, with increasing conversion and system viscosity, reduced group number and increased diffusion limitations may limit the reaction to contiguous molecules. When elevated temperatures endow these cyanate groups with larger free space and higher energy to rotate to positions in close proximity to other cyanate groups on the same molecule, the formation of an internal cycle may result. This should be true, especially at high conversions and high nanorod loadings, because the intracyclization between two molecules under such conditions is energy-beneficial compared with cyclotrimerization that is based on three-body collisions.

The effect of the addition of monofunctional monomers on the intracyclization of dicyanates has been considered by Li and Simon.[34] They reported that increasing concentrations of monofunctional monomers in dicyanates caused an increase in sol content in the cured samples. Analysis of mass spectra for the extracted sols indicated the presence of two primary species: the dimer formed by trimerization between a monofunctional monomer and a difunctional monomer (63.7%), and the trimer

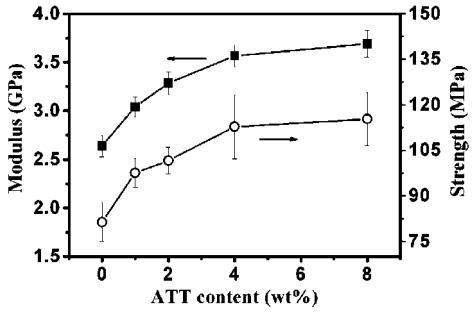

Figure 9. Effect of adding ATT nanorods on (■) the modulus and (○) the strength of CE resins.

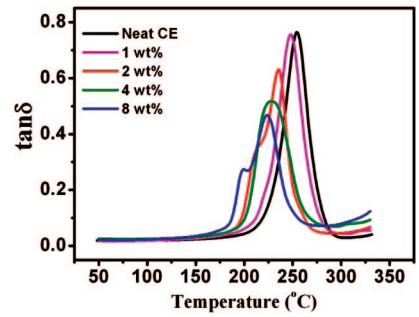

Figure 10. DMA damping spectra for the neat resin and nanocomposites.

of three monofunctional monomers (35.4%). No unreacted monomers were detected in the extracted sols. Modeling of 3-D molecular structures suggested that for bisphenol M and bisphenol A dicyanates, monomer cyclization was favorable, as opposed to oligomer cyclization. Unlike that example, however, the monofunctional species in the current work primarily originate as the product of reaction between dicyanates and amine groups grafted on the nanorod. These monofunctional species are very restricted around the nanorod. Thus, trimerization by reaction of three monofunctional monomers is difficult, especially at higher conversions. Consequently, delayed gelation is more likely to result from the formation of dimers formed by reaction of cyanate groups on the nanorod with two cyanate groups from the same dicyanate or oligomer. This is consistent with the conclusions of Gupta and Macosko,[33] who suggested that the delayed gelation behavior primarily originated from diffusion limitation and steric hindrance, which restricted reactions to localized regions.

Altogether, the addition of modified ATT nanorods to the CE monomer significantly affected the formation of organic networks. First, the amine groups on the nanorod surface reduced the cure temperature and shortened the cure time. Second, the addition of nanorods elevated the system viscosity and decreased the diffusion rate of functional groups. Finally, the introduction of amine groups increased the fraction of monofunctional species in the system, resulting in the reduction of cross-link density. Such changes in network structures will undoubtedly affect the macroscopic mechanical properties of CE nanocomposites.

3.3. Mechanical Properties of Cyanate Ester Nanocomposites. The modulus E_f and strength σ_f values for all samples were obtained from the flexural force−deformation curves and are plotted in Figure 9, where each point represents at least four replicates. For the neat CE resin, the E_f and σ_f values were 2.64 GPa and 81.35 MPa, which is consistent with earlier reports. The addition of 4 wt % nanorods increased the E_f and σ_f by 40 and 42% (3.57 GPa and 112.78 MPa). However, further increases in the particle loading to 8 wt % resulted in only modest increases in E_f and σ_f (from 3.57 to 3.69 GPa and from 112.78 to 115.33 MPa for σ_f). A similar trend was recently reported,[5a] and the phenomenon was attributed to increased free volume and decreased cross-link density. We attempt to elucidate the responsible mechanisms in light of the variation of the nanocomposite hybrid network structures.

Particle networks and interfacial interactions are often cited as the two primary factors that dominate the mechanical properties of polymer nanocomposites, although a consensus has not yet been reached. In previous work,[16b] interfacial interaction was shown to influence the mechanical reinforcement of nanocomposites strongly at loadings that were insufficient at forming percolated particle networks. Likewise, we assert that the increases in E_f and σ_f observed here stem from covalent bonding between nanorods and organic networks. This assertion is supported by the damping spectra. Figure 10 shows the effect of nanorods on the loss factor tan δ of the neat CE resin and the nanocomposites. The peak height of T_g dispersions markedly decreased with increasing nanorod loadings. Studies have suggested that the relative heights in T_g dispersions were inversely proportional to the volume fraction of confined segments in the interface layer.[35] This implies that increased nanorod loadings increase the covalent bonding between the nanorod and the matrix, which is also reflected in the variation in the widths of T_g dispersions. With increasing volume fraction of confined segments, the relaxation of segments at different sites in the system will span a wider temperature range. Those segments in the immediate vicinity of nanorods experience greater confinement, and thus their relaxation occurs at higher temperatures. In contrast, less-confined segments that are distant from the nanorods will exhibit relaxation behavior similar to that of the bulk. This insight is consistent with the results shown in Figure 10, in which a gradual broadening in T_g dispersion with increasing nanorod loadings is evident, particularly for the 8 wt % sample. Nevertheless, such an increased confinement effect seems to contradict the observed decreases in T_g (tan δ peak temperature). The incorporation of nanoparticles can cause the T_g to increase, decrease, or remain constant, depending on the dispersion status of particles and the interfacial interaction (strong, weak, or repulsive). As shown above, the dispersion of ATT nanorods in the CE resin is homogeneous, and few large aggregates were observed. The reduced T_g values thus arise from the reduced network density rather than the aggregates of nanorods, which is further confirmed by the shoulder peaks at the low temperature side of T_g dispersions. The similar phenomenon also appeared in the damping spectra of POSS/epoxy nanocomposites,[35c] where it was attributed to the effect of unreacted moieties on the segmental motion. For the ATT/CE nanocomposites, the relaxation behavior of CE networks is associated not only with the confinement effect of ATT nanorods but also with the network density. It is not surprising that more segments relax at lower temperature with decreasing network confinement. In this regard, the present results apparently underscore the importance of elevating stress transfer efficiency (covalent bonding) to achieve mechanical reinforcement.

Covalent bonding between nanorods and CE networks can be detected by FTIR spectroscopy. Figure 11 shows the in situ FTIR spectra of the neat CE resin and the 8 wt % ATT/CE nanocomposite at different temperatures. For these measurements, we prepared the 8 wt % sample by shearing at 90 °C for 1 h, soaking in a vacuum oven for 1 h to remove residual air, and encapsulating the mixture between two NaCl plates for FTIR spectroscopy. Prior to the cure, two strong bands appear at 2235 and 2268 cm^{-1} for the neat CE resin and the nanocomposite, which are assigned to the stretching vibration of C≡N groups.[36] After curing at 170 °C for 2 h, the C≡N absorbance bands for the nanocomposite nearly disappear, while the C≡N bands for the neat CE resin remain discernible. The

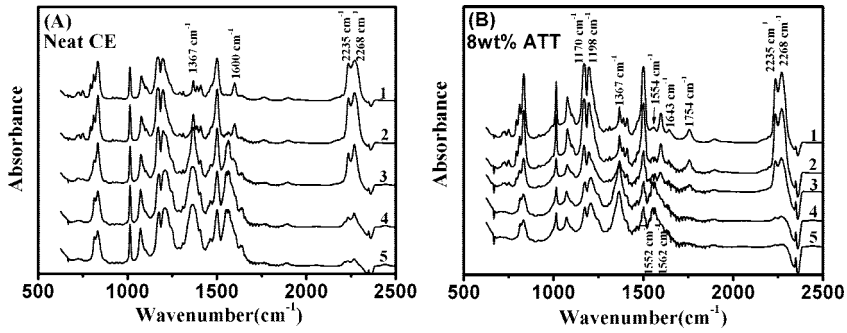

Figure 11. In situ FTIR measurements of cure reactions for (A) the neat CE resin and (B) the 8 wt % nanocomposite. The FTIR spectra in A and B were obtained (1) after melting at 90 °C, (2) after 1 h at 90 °C, (3) after 1 h at 120 °C, (4) after 2 h at 170 °C, and (5) after 2 h at 200 °C.

peak area of C≡N bands is customarily used to study the cure kinetics of CE resins.[37] The more rapid reduction in peak area of C≡N bands for the nanocomposite relative to that of the neat resin reflects the catalytic effect of the nanorods, which is also consistent with the DSC results (Figure 5). The characteristic absorptions of triazine rings appear at 1367 and 1560 cm^{-1} and drastically increase with the progress of cure reactions, together with the increasing stretching band of C−O−C at 1198 cm^{-1}. These features resemble previously reported results.[37] However, the appearance of a weak band at 1554 cm^{-1} for the nanocomposite prior to the cure is absent in the spectrum of the neat resin. (See curve 1 in Figure 11A,B). The weak band presumably originates from sources other than triazine ring formation. For example, the amide II absorption occurs between 1542 and 1559 cm^{-1}, and the bending vibration of NH appears at 1549 cm^{-1}.[38] However, the characteristic absorption of triazine rings at 1367 cm^{-1} indicates that it is plausible to assign the weak band to the triazine ring. A comparison of the relative peak heights of the 1367 cm^{-1} bands of the two samples shows that the nanocomposite exhibits a stronger absorption at 1367 cm^{-1} than does the neat resin, which indicates that limited cyclotrimerization can occur even at 90 °C, primarily because of the presence of amine groups.

Catalysis of cyanate cyclotrimerization by amine groups occurs by an amine−cyanate reaction,[31] which causes the linkage between inorganic particles (or particle networks) and organic networks, and also results in the formation of isoureas. The characteristic absorption of an isourea appears at 1643 cm^{-1}, although interference may arise from the stretching vibration of urea carbonyl groups (urea C═O) at 1647 cm^{-1}.[38] Urea bonds are undoubtedly present in organic molecules grafted onto the nanorod surface, which arise from isocyanate−amine reactions. Nevertheless, the detection of a characteristic absorption at 1754 cm^{-1} in the FTIR spectra of the nanocomposite would confirm the formation of an isourea, which is similar to the vibration band of C═NH at 1745 cm^{-1} that was observed in a recent report.[37a]

During the cure of dicyanates containing ATT nanorods, the reaction between amines and cyanates introduced cyanate groups to the nanorod surface, which allowed nanorods (or nanorod networks) to be incorporated into the organic networks. Several possible routes result in the formation of different hybrid network structures, as illustrated in Scheme 1. First, the grafting cyanate groups can react with two dicyanate monomers to form a triazine ring; subsequently, two cyanate groups linked with the triazine ring can react with other dicyanates, producing organic networks (route I (a) in Scheme 1). The reaction between primary amines and cyanates can take place at relatively low temperatures, although the reaction between secondary amines and cyanates is much slower and normally requires higher temperature. At higher temperatures, isoureas can be activated and react with cyanates to form triazine rings, along with the abstraction of a phenol or an amine (route II in Scheme 1). This would help explain the gradually weakened 1754 cm^{-1} band shown in Figure 11B, which reflects the reduction of isourea content in the system. Recently, Bauer et al. demonstrated that abstraction of phenols during the formation of triazine rings was favored over the abstraction of amines.[31] The abstraction of phenols in the present systems effectively tethers the triazine rings to the nanorods and enhances the interfacial bonding. The remaining phenols either (a) are incorporated into the organic networks as pendant terminals by the cyanate groups or (b) form oligomers because of the increasing viscosity of the system.

In the second route, the branched structure or networks formed by those cyanate groups tethered to nanorods cause space hindrance that restricts the accessibility of other cyanate groups. In this context, intracyclization with a single dicyanate will become possible (route III in Scheme 1), which results in the formation of linear or branched structures (the defects of organic networks) and thus reduces the T_g of nanocomposites. In the third route, the comparison of the absorption strength at 1554 cm^{-1} of the neat resin and nanocomposite (e.g., curve 3 in Figure 11A,B) reveals that after curing at 120 °C for 1 h, the number of triazine rings formed for the neat resin is much greater than that for the nanocomposite. This reflects the strong influence of viscosity on the diffusion rate of cyanate groups and the formation of triazine rings, which leads to the conclusion that a back-biting reaction occurs between the isourea and cyanate groups on the same molecule (route I (b) in Scheme 1).

On the basis of the above discussion, we propose a conceptional picture to illuminate the possible differences in interface and network structures, as well as the effects on mechanical properties. These differences originate from changes in the diffusion rate of cyanate groups, the shielding effect of branched (or network) structures, and the catalytic effect of amine groups. (See Figure 12.) For the neat resin, the diffusion rate of cyanate groups is not affected in the early stage of reaction but gradually declines with increasing system viscosity, causing the formation of small amounts of dimers or oligomers (Figure 12A). The addition of nanorods introduces aromatic amine groups to the system, which increases the mixture viscosity and accelerates the trimerization by forming isoureas. In the case of low ATT loadings (e.g., 1 or 2 wt %), increases in the viscosity are absent, and the effect on the diffusion rate of cyanate groups is weak. This allows large branched or network structures to form on the nanorod surface.

At this juncture, the key factor that affects the covalent linkage between nanorods and organic networks primarily arises from the space hindrance of contiguous branched or network structures on the nanorods. Once a branched or network structure forms at some site on a nanorod, it hinders the access of free cyanates to the contiguous cyanate group on the nanorod. This is similar to the findings or Gupta and Macosko,[33] where the shielding effect was reduced by the introduction of monofunc-

Scheme 1. Possible Mechanisms for the Formation of Organic Networks in ATT/CE Nanocomposites

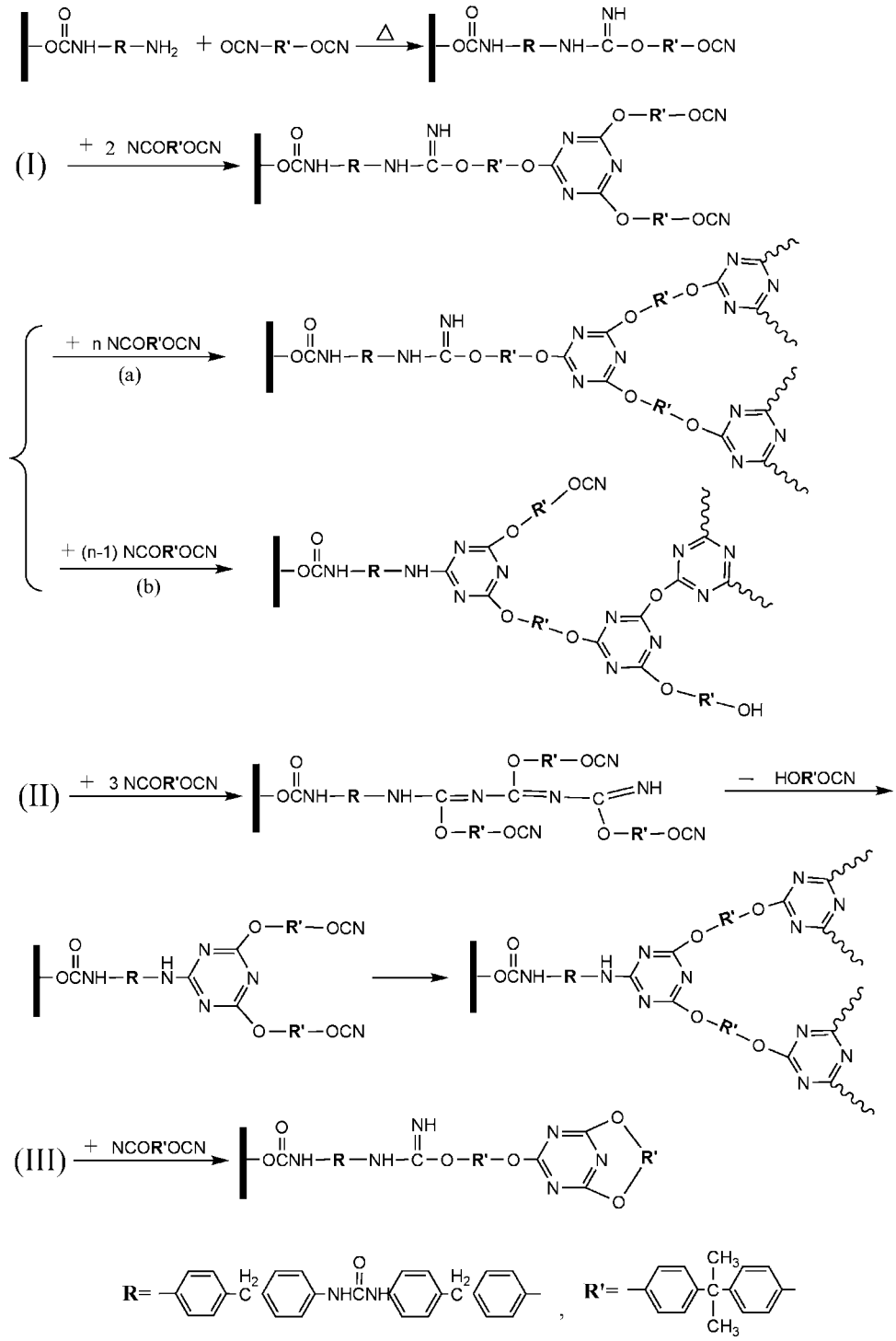

tional monomers. Even if the cyanate groups grafted on the nanorod grow simultaneously, some branches will experience space limitation, resulting in intracyclization. This will force cyanates on the nanorods to form more linear structures in the vicinity of nanorods, as depicted in Figure 12B. With increasing particle loadings, the system viscosity drastically increases, particularly after the formation of a percolated network, which significantly reduces the number of functional groups around a cyanate group. This favors the formation of linear structures and intracyclization, as shown Figure 12C. As a consequence, the effect of ATT nanorods on the microscopic structure of nanocomposites is naturally complex. On one hand, the high modulus of ATT increases the modulus and strength of the composites. On the other hand, the increased viscosity reduces the network density and impairs interfacial bonding on account of more linear structures and intracyclizations. It is thus plausible that the reinforcement saturation revealed in the 8 wt % nanocomposite (Figure 9) originates from a combination of these factors, including the adverse effect of percolated particle networks (increased viscosity and intracyclization, decreased organic network density, and interface interaction).

Figure 13 presents the fracture toughness K_{IC} of the neat resin and the nanocomposites. The toughness increases with nanorod loading, which is similar to the modulus and strength (Figure 9). For the neat resin, the K_{IC} is 0.94 MN/m$^{2/3}$, which is consistent with reported values.[22] The addition of 4 wt %

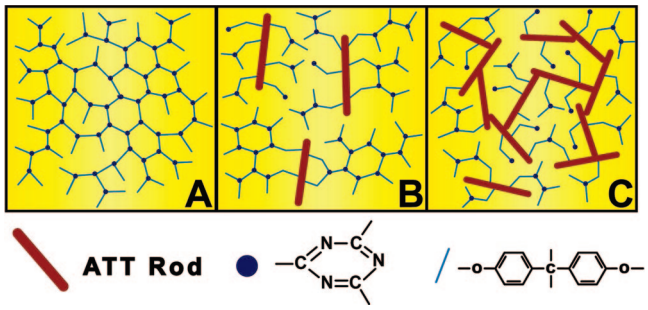

Figure 12. Conceptional picture of hybrid networks: (A) neat resin, (B) low particle contents, and (C) high particle contents.

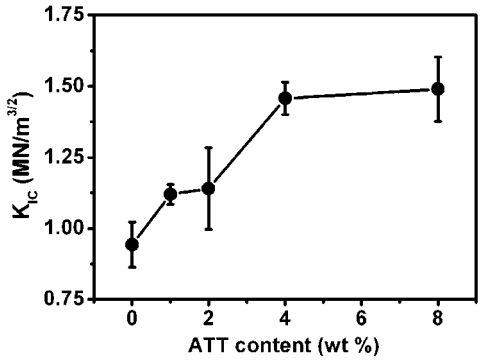

Figure 13. Effect of adding ATT nanorods on the fracture toughness of CE resins.

nanorods increases the K_{IC} value by 55% (1.46 MN/m$^{2/3}$) relative to the neat resin. However, further increases in nanorod loading (8 wt %) cause only a 3% increase. This trend is similar to the findings reported for systems containing layered silicates, although a minor difference is that the K_{IC} values for layered silicate nanocomposites begin to decrease after particle loadings exceed 3 wt %. Enhanced toughness has been attributed to increases in the surface area of particles and interaction with the advancing crack front. However, this explanation does not explain why the toughening effect diminishes at high particle loadings.

Molecular dynamics simulations have demonstrated that the mobility of nanoparticles is a key factor for the toughening of polymer materials.[39] Because the time scale for motion of nanoparticles is comparable to that of polymers, the motion of nanoparticles contributes to the formation of temporary cross-links between polymer chains and thus retards the propagation of cracks during deformation. This provides composites with an additional energy dissipation route. Such a toughening mechanism has been confirmed by experimental observations.[40] Nevertheless, the toughening mechanism is applicable to only the fracture of polymers in the rubbery state. For glassy polymers, consensus has not been reached, although particle toughening has been achieved to different extents.[41] Multiple models have been proposed to explain the phenomenon, including crack pinning, crack bridging, and debonding of particles as well as crack deflection.[42] Particle toughening of glassy polymers strongly depends on the polymer type, the size and shape of particles, and the particle−matrix interaction. For different polymers, both crack propagation resistance and particle migration capacity have been proposed to explain the observed toughness improvement. In previous work, crack propagation resistance, mobility of segments, and free volume fraction were asserted as three important factors that determine the fracture behavior of thermoplastic polyimide nanocomposites.[16b] These factors can also be invoked to explain the fracture behavior of ATT/CE nanocomposites, provided that the effect of hybrid network structures is included in the analysis of fracture mechanisms.

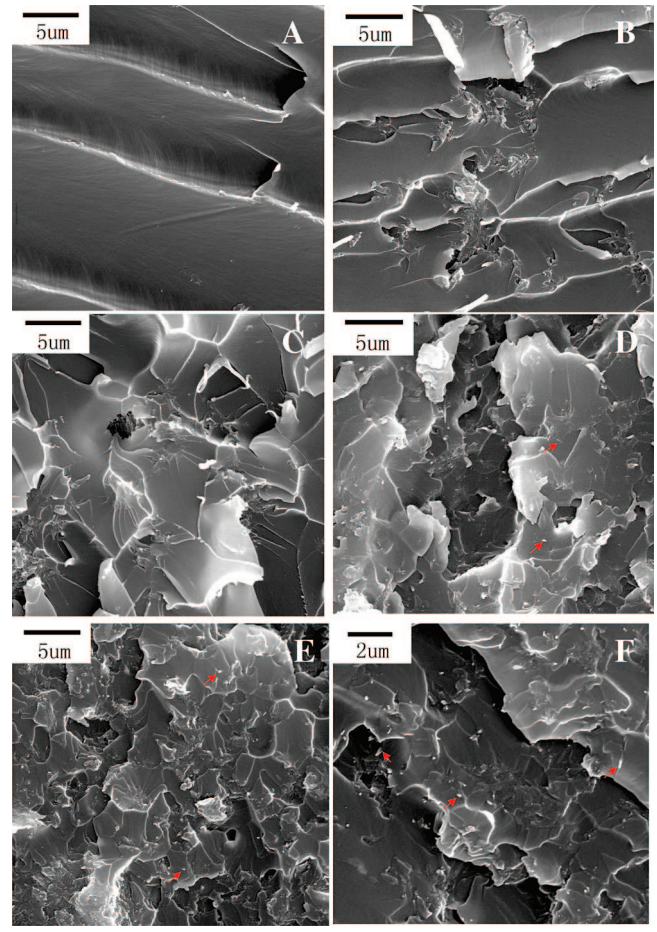

Figure 14. SEM fractographs of the neat CE resin and ATT−CE nanocomposites: (A) neat resin and nanocomposites, (B) 1 wt % ATT, (C) 2 wt % ATT, (D) 4 wt % ATT, (E) 8 wt % ATT, and (F) amplified 8 wt % ATT for clearer observation of the ATT−CE interface. The stubs marked by red arrows are ATT nanorods partially imbedded in the CE resin.

The contribution of nanorods to crack propagation resistance is manifested in SEM fractographs of the nanocomposites. As shown in Figure 14A, smooth ribbon structures are the main feature of the fracture surface of the neat CE resin, as previously reported.[22] However, the addition of nanorods changed the morphology of the fracture surface. First, the size of ribbons becomes smaller, and the shape gradually becomes irregular with increasing nanorod loadings. Overall morphological variations for these samples can be observed from the fractographs with low modifications. (See Figure S2 in the Supporting Information.) Similar phenomena were reported for thermoplastic systems, and it was concluded that stronger nanorod−matrix bonding effectively resisted crack propagation.[16b] With increased particle loadings, the frequency of nanoparticle−crack interaction increases, thus increasing the fracture toughness. In this context, interface control becomes critical. Increased covalent bonding and entanglements with the bulk provide greater resistance to cracks along the nanoparticle surface. Whereas amine groups on the nanorod surface improved the bonding in the present CE systems, they induced increased intracyclizations and led to the formation of dimers or oligomers. The latter species impaired the linkage between inorganic particles (or networks) and organic networks and thus mitigated the toughness enhancement. This was especially true at higher nanorod loadings, for which the presence of more short chains or branches not only mitigated the network density of CE resins

but also weakened the linkage between particles and organic networks. As a consequence, the slight toughness increase in the 8 wt % sample reflects a balance between the increasing number of nanorods and the reduced interfacial linkage between particles and organic networks.

The analysis is confirmed by further observation of the etched fracture morphology of the nanocomposites. At low ATT loadings, discerning ATT nanorods on the fracture surface is somewhat difficult because of the interference of pleats and protuberances (Figure 14B,C). For instance, some protuberances that were observed in the neat resin (Figure 14A) make it difficult for us to distinguish nanorods dispersed in the 1 and 2 wt % samples. For the 4 and 8 wt % samples, however, ATT nanorods are clearly visible (Figure 14D,E) and exhibit some dispersion homogeneity of nanorods. It is important to consider their random orientation in the matrix upon assessing the dispersion status of ATT. Those nanorods that are parallel to the fracture direction are presumedly imbedded under the smooth surface and are invisible because the covalent bonding at the interface forces cracks to propagate preferentially in the resin phase. This is the primary cause of the fracture surface becoming increasingly irregular with the addition of nanorods. Different from the case of thermoplastic polymer nanocomposites,[16b] in which plastic deformation takes place during fracture and allows nanorods to orient along the force direction, the orientation of nanorods in cured CE composites is relatively difficult because of the confinement of cross-linked networks. During the fracture, when the imposed force exceeds the strength of the nanorods that are vertical to the fracture direction, most of them are fractured rather than pulled out from the matrix because of strong interface bonding. This explains why we can observe only some light points or stubs of nanorods on the fracture surface. Nevertheless, a few slightly long nanorod stubs can be found from the amplified fracture surface of the 8 wt % sample (Figure 14F), which is consistent with the weakened interface bonding at high nanorod loadings mentioned above.

The smooth ribbon features that characterize the neat resin fracture surface gradually diminish with increasing solid loadings and evolve into smaller fragments. These fragments and cracks also appear in some deeper places on the fracture surface. The phenomenon is clearly manifested in the 8 wt % sample, as shown in Figure 14E. Increased nanorod loadings induce more cracks because of the increased free volume fraction. The latter increases the mobility of segments, enhancing the endurance of organic networks to an external stress. However, the free volumes aggregate into cavities and develop into cracks during deformation. Increased free volume fractions in polymer nanocomposites have been reported elsewhere.[43] In this regard, the comparison of measured and calculated densities for different samples can illustrate the presence of free volume in nanocomposites. As shown in Figure 15A, measured results increasingly deviate from the values that were calculated in light of the rule of mixture, which is an indicator of the free volume in CE nanocomposites increasing with increasing ATT content. Additionally, thermogravimetric experiments can reflect the effect of free volume on the thermal stability of nanocomposites. (See Figure 15B and Table 1). The $T_{d,10\%}$ for the neat resin is 476 °C, and the addition of nanorods does not appreciably affect the thermal stability, despite slight decreases (~9 °C for the 8 wt % sample) in $T_{d,10\%}$ with increasing nanorod loadings. Note that the residual weights of all nanocomposites at temperatures of >500 °C are less than that of the neat resin. This is consistent with previous observations[16b] in which the phenomenon was attributed to the increasing free volume fractions in the systems.

4. Conclusions

The design and optimization of thermosetting polymer nanocomposites requires a fundamental understanding of the structure/property relationship. Weak interparticle interactions of rodlike ATT nanoparticles afford convenient dispersion in polymers, which permits the systematic study of the evolution of microstructures and the correlation with the behavior of bulk nanocomposites. To establish such a correlation, we prepared ATT/CE nanocomposites that contained different particle loadings in which the surface of ATT nanorods was modified with aromatic diisocyanate (MDI) and diamine (MDA). Sedimentation experiments displayed a good dispersion stability of nanorods in CE monomers for up to 2 h or more, which ensures homogeneous distribution of nanorods in the CE nanocomposites. Rheological measurements revealed typical thixotropic behavior for ATT/CE monomer mixtures as particle loadings beyond 2 wt %. On the basis of the dynamic measurements, the percolation threshold of the mixtures was estimated to be 8.5 wt %. However, the threshold was reduced in the cured nanocomposites on the basis of TEM observations. We assert that a good affinity of nanorods for CE monomers enables the monomer to enter the inter-rod spacings of large aggregates readily. Furthermore, subsequent curing reactions exfoliate large aggregated nanorods, creating smaller aggregates or individual nanorods and thus homogenizing the particle size distribution in final nanocomposites.

The addition of nanorods also affected the formation of organic networks. On one hand, the amine groups grafted onto the nanorod surface accelerated the polycyclotrimerization of CE monomers, decreased the cure temperature, and shortened the gel time of the systems. On the other hand, the increased viscosity of the systems restricted the diffusion of functional groups and caused increased intracyclizations. In addition, the presence of amine groups reduced the functionality of the system, enhancing intracyclizations and reducing the organic network density.

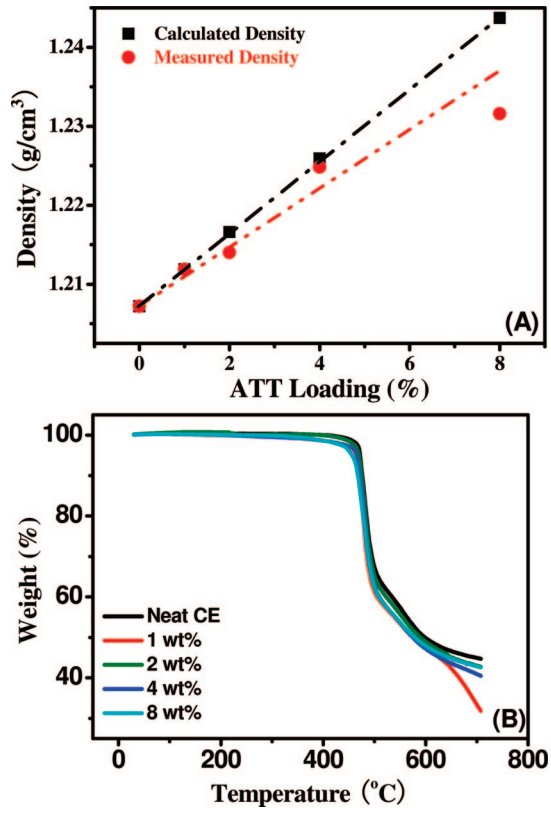

Figure 15. (A) Comparison of calculated and measured densities with a Mettler Toledo AL 204 balance and the density accessory (resolution: 10^{-3} g/cm^3). $\rho = (m_1/\rho_1 + m_2/\rho_2)^{-1}$, where m_1 and m_2 are the weight fractions of ATT and CE resin. $\rho_1 = 2.0$ g/cm^{-3} and $\rho_2 = 1.2072$ g/cm^3 are the densities of ATT and CE resin, respectively. (B) TGA curves of the neat resin and nanocomposites.

The modulus, strength, and toughness of nanocomposites increased 40−55% relative to the neat resin. However, the increases at high particle loadings (e.g., 8 wt %) were negligible. The interfacial stress transfer efficiency increased because of the reaction between amine and cyanate groups, although the structure of the interfacial layers was altered at increased particle loadings. Once cyanate groups were grafted onto the nanorods by amine−cyanate reactions, their mobility drastically decreased; therefore, the probability of forming linear or branching structures by intracyclizations correspondingly increased. Furthermore, a branch structure tethered to the nanorod surface sterically hindered the access of other functional groups to contiguous cyanate groups, thus fomenting the formation of linear, less-branched structures. With increasing system viscosity, the interaction between interfacial layers and the bulk was impaired, particularly at high particle loadings. The variation in the interfacial structure likewise weakens the resistance to crack propagation during deformation. Increased free volume fractions were associated with increasing particle loadings, which contributed to cavity formation and cracking during fracture.

Acknowledgment. This work was supported by the National Basic Research Program of China (grant no. 2005CB623800), the NSF of China (grant nos. 50573014 and 50773012), and the Shanghai Basic Research Program (grant no. 05JC14002). We thank the reviewers for their constructive suggestions to this manuscript. H.L. and Y.Y. also acknowledge the support of the NSFC program "Excellence in Research Group" (grant no. 20221402).

Supporting Information Available: Dynamic rheological results, low magnification SEM fractographs of the neat resin and ATT−CE nanocomposites, and appearance of the neat resin and ATT−CE nanocomposites. This material is available free of charge via the Internet at http://pubs.acs.org.

References and Notes

(1) (a) Wen, J.; Wilkes, G. L. *Chem. Mater.* **1996**, *8*, 1667. (b) Jackson, C. L.; Bauer, B. J.; Nakatani, A. I.; Barnes, J. D. *Chem. Mater.* **1996**, *8*, 727. (c) Innocenzi, P.; Brusatin, G.; Babonneau, F. *Chem. Mater.* **2000**, *12*, 3726. (d) Mayer, C. R.; Thouvenot, R.; Lalot, T. *Chem. Mater.* **2000**, *12*, 257. (e) Peng, F. B.; Lu, L. Y.; Sun, H. L.; Wang, Y. Q.; Liu, J. Q.; Jiang, Z. Y. *Chem. Mater.* **2005**, *17*, 6790. (f) Schottner, G. *Chem. Mater.* **2001**, *13*, 3422.

(2) Vendamme, R.; Onoue, S. Y.; Nako, A.; Kunitake, T. *Nat. Mater.* **2006**, *5*, 494.

(3) (a) Haraguchi, K.; Li, H. J. *Angew. Chem., Int. Ed.* **2005**, *44*, 6500. (b) Haraguchi, K.; Takehisa, T. *Adv. Mater.* **2002**, *14*, 1120.

(4) Kharchenko, S. B.; Douglas, J. F.; Obrzut, J.; Grulke, E. A.; Migler, K. B. *Nat. Mater.* **2004**, *3*, 564.

(5) (a) Liang, K. W.; Li, G. Z.; Toghiani, H.; Koo, J. H.; Pittman, C. U., Jr *Chem. Mater.* **2006**, *18*, 301. (b) Zheng, S. X.; Ni, Y. *Macromolecules* **2007**, *40*, 7009. (c) Zucchi, I. A.; Galante, M. J.; Williams, R. J. J.; Franchini, E.; Galy, J.; Gerard, J. F. *Macromolecules* **2007**, *40*, 1274.

(6) Wilder, E. A.; Braunfeld, M. B.; Jinnai, H.; Hall, C. K.; Agard, D. A.; Spontak, R. J. *J. Phys. Chem. B* **2003**, *107*, 11633.

(7) Haraguchi, K.; Song, L. Y. *Macromolecules* **2007**, *40*, 5526.

(8) (a) Krishnamoorti, R. *MRS Bull.* **2007**, *32*, 341. (b) Li, J.; Ma, P. C.; Chow, W. S.; To, C. K.; Tang, B. Z.; Kim, J. K *Adv. Funct. Mater.* **2007**, *17*, 3207. (c) Schilling, T.; Jungblut, S.; Miller, M. A. *Phys. Rev. Lett.* **2007**, *98*, 108303. (d) Fan, Z. H.; Advani, S. G. *J. Rheol.* **2007**, *51*, 585.

(9) (a) Balberg, I.; Binenbaum, N.; Wagner, N. *Phys. Rev. Lett.* **1984**, *52*, 1465. (b) Bug, A. L. R.; Safran, S. A.; Webman, I. *Phys. Rev. Lett.* **1985**, *54*, 1412.

(10) Mackay, M. E.; Tuteja, A.; Duxbury, P. M.; Hawker, C. J.; Horn, B. V.; Guan, Z. B.; Chen, G. H.; Krishnan, R. S. *Science* **2006**, *311*, 1740.

(11) Brus, J.; Spirkova, M.; Hlavata, D.; Strachota, A. *Macromolecules* **2004**, *37*, 1346.

(12) Uhl, F. M.; Davuluri, S. P.; Wong, S. C.; Webster, D. C. *Chem. Mater.* **2004**, *16*, 1135.

(13) (a) Lamm, M. H.; Chen, T.; Glotzer, S. C. *Nano Lett.* **2003**, *3*, 989. (b) Sheng, Y. J.; Lin, W. J.; Chen, W. C. *J. Chem. Phys.* **2004**, *121*, 9693.

(14) (a) Lee, T. Y.; Bowman, C. N. *Polymer.* **2006**, *47*, 6057. (b) Chiou, B. S.; Raghavan, S. R.; Khan, S. K. *Macromolecules* **2001**, *34*, 4526.

(15) (a) Balazs, A. C.; Emrick, T.; Russell, T. P. *Science* **2006**, *314*, 1107. (b) Gupta, S.; Zhang, Q. L.; Emrick, T.; Balazs, A. C.; Russell, T. P. *Nat. Mater.* **2006**, *5*, 229. (c) Bansal, A.; Yang, H. C.; Li, C. Z.; Cho, K. W.; Benicewicz, B. C.; Kumar, S. K.; Schadler, L. S. *Nat. Mater.* **2005**, *4*, 693. (d) Moniruzzaman, M.; Chattopadhyay, J.; Billups, W. E.; Winey, K. I. *Nano Lett.* **2007**, *7*, 1178. (e) Mu, M.; Winey, K. I. *J. Phys. Chem. C* **2007**, *111*, 17923.

(16) (a) Xie, L.; Xu, F.; Qiu, F.; Lu, H. B.; Yang, Y. L. *Macromolecules* **2007**, *40*, 3296. (b) An, L.; Pan, Y. Z.; Chen, H. G.; Shen, X. W.; Lu, H. B.; Yang, Y. L. *J. Mater. Chem.* **2008**, *18*, 4928−4941. (c) Jose-Yacaman, M.; Rendon, L.; Arenas, J.; Puche, M. C. S. *Science* **1996**, *273*, 223. (d) Xue, S. Q.; Reinholdt, M.; Pinnavaia, T. J. *Polymer* **2006**, *47*, 3344. (e) Sampson, P; Parker, D.; Ruff, D. U.S. Patent 6130179.

(17) (a) Frenkel, D.; Lekkerkerker, H. N. W.; Stroobants, A. *Nature* **1988**, *332*, 822. (b) Lekkerkerker, H. N. W.; Stroobants, A. *Nature* **1998**, *393*, 305. (c) Wong, E. W.; Sheehan, P. E.; Lieber, C. M. *Science* **1997**, *277*, 1971. (d) Huynh, W. U.; Dittmer, J. J.; Alivisatos, A. P. *Science* **2002**, *295*, 2425. (e) Zheng, X. Y.; Forest, M. G.; Vaia, R.; Arlen, M.; Zhou, R. H. *Adv. Mater.* **2007**, *19*, 4038. (f) Maeda, H.; Maeda, Y. *Nano Lett.* **2007**, *7*, 3329. (g) Li, L. S.; Walda, J.; Manna, L.; Alivisatos, A. P. *Nano Lett.* **2002**, *2*, 557. (h) Mohraz, A.; Moler, D. B.; Ziff, R. M.; Solomon, M. J. *Phys. Rev. Lett.* **2004**, *92*, 155503. (i) Nie, Z. H.; Fava, D.; Kumacheva, E.; Zou, S.; Walker, G. C.; Rubinstein, M. *Nat. Mater.* **2007**, *6*, 609. (j) Schilling, T.; Jungblut, S.; Miller, M. A. *Phys. Rev. Lett.* **2007**, *98*, 108303.

(18) Capadona, J. R.; Berg, O. V. D.; Capadona, L. A.; Schroeter, M.; Rowan, S. J.; Tyler, D. J.; Weder, C. *Nature Nanotechnol.* **2007**, *2*, 765.

(19) (a) Lu, H. B.; Shen, H. B.; Song, Z. L.; Shing, K. S.; Wei, T.; Nutt, S. *Macromol. Rapid Commun.* **2005**, *26*, 1445. (b) Chen, X. Q.; Xu, J. J.; Lu, H. B.; Yang, Y. L. *J. Polym. Sci., Part B: Polym. Phys.* **2006**, *44*, 2112.

(20) (a) Fang, T.; Shimp, D. *Prog. Polym. Sci.* **1995**, *20*, 61. (b) Reghunadhan Nair, C. P.; Mathew, D.; Ninan, K. N. *Adv. Polym. Sci.* **2001**, *155*, 1.

(21) Maya, E. M.; Snow, A. W.; Buckley, L. J *Macromolecules* **2002**, *35*, 460. (b) Kim, Y. S.; Kim, S. C *Macromolecules* **1999**, *32*, 2334. (c) Marieta, C.; Schulz, E.; Irusta, L.; Gabilondo, N.; Tercjak, A.; Mondragon, I. *Compos. Sci. Technol.* **2005**, *65*, 2189. (d) Lin, C. H. *Polymer* **2004**, *45*, 7911. (e) Hamerton, I.; Takeda, S. *Polymer* **2000**, *41*, 1647. (f) Barton, J. M.; Hamerton, I.; Jones, J. R.; Stedman, J. C. *Polymer* **1996**, *37*, 4519. (g) Hwang, J. W.; Park, S. D.; Cho, K.; Kim, J. K.; Park, C. E.; Oh, T. S. *Polymer* **1997**, *38*, 1835. (h) Srinivasan, S. A.; McGrath, J. E. *Polymer* **1998**, *39*, 2415.

(22) (a) Che, J. F.; Chan-Park, M. B. *Adv. Funct. Mater.* **2008**, *18*, 888. (b) Liang, K. W.; Toghiani, H.; Li, G. Z.; Pittman, C. U. *J. Polym. Sci., Part A: Polym. Chem.* **2005**, *43*, 3887. (c) Ganguli, S.; Dean, D.; Jordan, K.; Price, G.; Vaia, R. *Polymer* **2003**, *44*, 1315.

(23) (a) Liang, Y.; Hilal, N.; Langston, P.; Starov, V. *Adv. Colloid Interface Sci.* **2007**, *135−35*, 151. (b) Smith, W. E.; Zukoski, C. F. *J. Colloid Interface Sci.* **2006**, *304*, 348.

(24) Khair, A. S.; Brady, J. F. *J. Rheol.* **2008**, *52*, 165.

(25) (a) Huang, Y. Y.; Ahir, S. V.; Terentjev, E. M. *Phys. Rev. B* **2006**, *73*, 125422. (b) Fang, Z. H.; Advani, S. G. *J. Rheol.* **2007**, *51*, 585. (c) Jogun, S. M.; Zukoski, C. F. *J. Rheol.* **1999**, *43*, 847. (d) Li, S. P.; Hou, W. G.; Sun, D. J.; Guo, P. Z.; Jia, C. X. *Langmuir* **2003**, *19*, 3172. (e) Starck, P.; Mosse, W. K. J.; Nicholas, N. J.; Spiniello, M.; Tyrrell, J.; Nelson, A.; Qiao, G. G.; Ducker, W. A. *Langmuir* **2007**, *23*, 7587.

(26) (a) Solomon, M. J.; Boger, D. V. *J. Rheol.* **1998**, *42*, 929. (b) Barnes, H. A. *J. Non-Newtonian Fluid Mech.* **1997**, *70*, 1. (c) Winter, H. H.; Chambon, F. *J. Rheol.* **1986**, *30*, 367. (d) He, Y. Y.; Boswell, P. G.; Buhlmann, P.; Lodge, T. P *J. Phys. Chem. B,* **2007**, *111*, 4645.

(27) (a) Meuer, S.; Oberle, P.; Theato, P.; Tremel, W.; Zentel, R. *Adv. Mater.* **2007**, *19*, 2073. (b) Zhang, Z. X.; van Duijneveldt, J. S. *J. Chem. Phys.* **2006**, *124*, 154910.

(28) Vaia, R. A.; Giannelis, E. P. *Macromolecules* **1997**, *30*, 8000.

(29) Wooster, T. J.; Abrol, S.; MacFarlane, D. R. *Polymer* **2004**, *45*, 7845.

(30) (a) Ganguli, S.; Dean, D.; Jordan, K.; Price, G.; Vaia, R. *Polymer* **2003**, *44*, 6901. (b) Dean, D.; Walker, R.; Theodore, M.; Hampton, E.; Nyairo, E. *Polymer* **2005**, *46*, 3014.

(31) Bauer, J.; Bauer, M. *Macromol. Chem. Phys.* **2001**, *202*, 2213.

(32) Wang, F. L.; Hong, J. L. *Polymer* **1998**, *39*, 4319.

(33) Gupta, A. M.; Macosko, C. W. *Macromolecules* **1993**, *26*, 2455.

(34) (a) Li, Q. X.; Simon, S. L. *Macromolecules* **2007**, *40*, 2246. (b) Li, Q. X.; Simon, S. L. *Macromolecules* **2008**, *41*, 1310.

(35) (a) Burnside, S. D.; Giannelis, E. P. *J. Polym. Sci., Part B: Polym. Phys.* **2000**, *38*, 1595. (b) Rao, Y. Q.; Pochan, J. M. *Macromolecules* **2007**, *40*, 290. (c) Fu, B. X.; Namani, M.; Lee, A. *Polymer* **2003**, *44*, 7739.
(36) Grenier-Loustalot, M. F.; Lartigau, C.; Metras, F.; Grenier, P. *J. Polym. Sci., Part A: Polym. Chem.* **1996**, *34*, 2955.
(37) (a) Lin, C. H. *Polymer* **2004**, *45*, 7911. (b) Lin, R. H.; Lu, W. H.; Lin, C. W. *Polymer* **2004**, *45*, 4423.
(38) (a) Wang, S. K.; Sung, C. S. P. *Macromolecules* **2002**, *35*, 877. (b) Queiroz, D. P.; de Pinho, M. N.; Dias, C. *Macromolecules* **2003**, *36*, 4195. (c) Vanjinathan, M.; Nasar, A. S. *J. Polym. Sci., Part A: Polym. Chem.* **2008**, *46*, 713.
(39) Gersappe, D. *Phys. Rev. Lett.* **2002**, *89*, 058301.
(40) (a) Shah, D.; Maiti, P.; Gunn, E.; Schmidt, D. F.; Jiang, D. D.; Batt, C. A.; Giannelis, E. R. *Adv. Mater.* **2004**, *16*, 1173. (b) Shah, D.; Maiti, P.; Jiang, D. D.; Batt, C. A.; Giannelis, E. P. *Adv. Mater.* **2005**, *17*, 525. (c) Zhou, T. H.; Ruan, W. H.; Rong, M. Z.; Zhang, M. Q.; Mai, Y. L. *Adv. Mater.* **2007**, *19*, 2667.
(41) Referring to ref 16b and references cited there.
(42) (a) Tanniru, M.; Yuan, Q.; Misra, R. D. K. *Polymer* **2006**, *47*, 2133. (b) Fiedler, B.; Gojny, F. H.; Wichmann, M. H. G.; Nolte, M. C. M.; Schulte, K. *Compos. Sci. Technol.* **2006**, *66*, 3115. (c) Cotterell, B.; Chia, J. Y. H.; Hbaieb, K. *Eng. Fract Mech.* **2007**, *74*, 1054. (d) Johnsen, B. B.; Kinloch, A. J.; Mohammed, R. D.; Taylor, A. C.; Sprenger, S. *Polymer* **2007**, *48*, 530.
(43) (a) Mackay, M. E.; Dao, T. T.; Tuteja, A.; Ho, D. L.; Horn, B. V.; Kim, H. C.; Hawker, C. J. *Nat. Mater.* **2003**, *2*, 762. (b) Merkel, T. C.; Freeman, B. D.; Spontak, R. J.; He, Z.; Pinnau, I.; Meakin, P.; Hill, A. J. *Science* **2002**, *296*, 519. (c) Merkel, T. C.; Freeman, B. D.; Spontak, R. J.; He, Z.; Pinnau, I.; Meakin, P.; Hill, A. J. *Chem. Mater.* **2003**, *15*, 109. (d) Park, I.; Peng, H. G.; Gidley, D. W.; Xue, S. Q.; Pinnavaia, T. J. *Chem. Mater.* **2006**, *18*, 650.

MA800819S